

# Unprecedented large-scale aquifer recovery through human intervention

Received: 6 February 2025

Accepted: 23 July 2025

Published online: 07 August 2025

 Check for updates

Di Long <sup>1,2,15</sup> ✉, Yuancheng Xu <sup>1,2,15</sup>, Yingjie Cui <sup>1,2,15</sup>, Yanhong Cui<sup>1,2</sup>, James J. Butler Jr.<sup>3</sup>, Liang Dong<sup>1,2</sup>, Longfeng Wang<sup>4</sup>, Dongyong Liu<sup>4</sup>, Yoshihide Wada <sup>5</sup>, Litang Hu <sup>6</sup>, Guoying Bai<sup>7</sup>, Binghua Li<sup>8</sup>, Shufang Wang<sup>9</sup>, Xizhi Nong <sup>1,10</sup>, Yang Cai<sup>11</sup>, Chunsheng Cheng<sup>11</sup>, Yuhan Mu<sup>11</sup>, Yu Qiao<sup>12</sup>, Jianhua Wang <sup>13</sup>, Hao Wang<sup>13</sup> & Bridget R. Scanlon <sup>14</sup>

Groundwater depletion is a critical global challenge, particularly in intensively cultivated drylands, with few documented cases of successful recovery. Here, we report a striking reversal of long-term groundwater decline in the North China Plain, one of the world's most severely depleted aquifers. Based on a comprehensive analysis of groundwater levels from over 2000 monitoring wells spanning the past two decades, we show that groundwater levels have risen at an average rate of  $-0.7 \text{ m year}^{-1}$  since 2020, surpassing 2005 levels by 2024. This recovery is driven by a combination of large-scale surface water diversion from the humid south and stringent groundwater pumping regulations, further amplified by wet years (e.g., 2021). From 2005 to 2023, these policies reduced annual groundwater abstraction by  $-12 \text{ km}^3$  and increased environmental water allocations to over  $7 \text{ km}^3$  since 2021, promoting aquifer recharge and restoring environmental flows. Our findings demonstrate that rapid, large-scale groundwater recovery is achievable through integrated water management and targeted policy interventions across extensive regions ( $-130,000 \text{ km}^2$ ).

Groundwater depletion is a critical global challenge<sup>1–4</sup>, particularly in intensively cultivated drylands<sup>5</sup>. Continued declines in groundwater levels will have wide-ranging impacts, including land subsidence<sup>6,7</sup>, the desiccation of rivers and wetlands<sup>8,9</sup>, seawater intrusion<sup>10</sup>, intense economic pressure on rural communities<sup>11</sup>, and threats to the viability of global food supplies<sup>1</sup>. To mitigate groundwater depletion, various strategies have been implemented worldwide, such as reduced groundwater abstraction<sup>12,13</sup>, substitution of groundwater

pumping with surface water from reservoirs<sup>14</sup>, managed aquifer recharge (MAR)<sup>12,15,16</sup>, and inter-basin water diversions<sup>17–19</sup>. Despite these efforts, a recent study found that rapid groundwater level declines ( $>0.5 \text{ m year}^{-1}$ ) remain widespread, with only a small fraction of globally productive aquifers showing signs of recovery (aquifers with rising trends  $>0.2 \text{ m year}^{-1}$  constituting  $-6\%$  over the past two decades)<sup>5</sup>. Cases of groundwater recovery, when reported, are often spatially limited and exhibit only modest rates of recovery (e.g.,

<sup>1</sup>State Key Laboratory of Hydrosphere Science and Engineering, Department of Hydraulic Engineering, Tsinghua University, Beijing, China. <sup>2</sup>Key Laboratory of Hydrosphere Sciences of the Ministry of Water Resources, Tsinghua University, Beijing, China. <sup>3</sup>Kansas Geological Survey, University of Kansas, Lawrence, KS, USA. <sup>4</sup>China Institute of Geo-Environment Monitoring, Beijing, China. <sup>5</sup>Biological and Environmental Science and Engineering Division, King Abdullah University of Science and Technology, Thwal, Saudi Arabia. <sup>6</sup>College of Water Sciences, Beijing Normal University, Beijing, China. <sup>7</sup>Beijing Hydrology Center, Beijing, China. <sup>8</sup>Beijing Water Science and Technology Institute, Beijing, China. <sup>9</sup>Beijing Institute of Geological Environment Monitoring, Beijing, China. <sup>10</sup>College of Civil Engineering and Architecture, Guangxi University, Nanning, China. <sup>11</sup>Information Center, Ministry of Water Resources, Beijing, China. <sup>12</sup>China South-to-North Water Diversion Corporation Limited, Beijing, China. <sup>13</sup>State Key Laboratory of Water Cycle and Water Security, China Institute of Water Resources and Hydropower Research, Beijing, China. <sup>14</sup>Bureau of Economic Geology, Jackson School of Geosciences, University of Texas at Austin, Austin, TX, USA. <sup>15</sup>These authors contributed equally: Di Long, Yuancheng Xu, Yingjie Cui. ✉ e-mail: [dlong@tsinghua.edu.cn](mailto:dlong@tsinghua.edu.cn)

Mancha Occidental aquifer (Spain)<sup>20</sup>, Abbas-e Sharghi basin (Iran)<sup>14</sup>, Eastern Malwa Plateau alluvial aquifer (India)<sup>21</sup>, Bangkok basin (Thailand)<sup>13</sup>, Taiyuan basin (China)<sup>19</sup>, and parts of California and Arizona (US)<sup>18</sup>; Fig. 1). Cultivated drylands are particularly vulnerable to rapid and accelerating groundwater level declines due to inadequate management strategies<sup>5</sup>. In this context, the North China Plain (NCP), an intensively cultivated region spanning ~130,000 km<sup>2</sup>, presents a compelling case study. Here, we use the NCP as an example to demonstrate the feasibility of achieving rapid groundwater recovery (-0.7 m year<sup>-1</sup>) at an unprecedented spatial scale through ongoing human intervention.

The NCP, which forms the plain portion of the Hai River basin (HRB), has been identified as a global hotspot for groundwater depletion<sup>1</sup>. This region, which is responsible for ~10% of China's grain production, supports a population of ~130 million people and is characterized by severely limited water resources, with <500 m<sup>3</sup> of renewable water resources available per capita annually<sup>22,23</sup>. To meet the escalating demands of socioeconomic development, groundwater in the NCP has been heavily exploited. By the early 2000s, groundwater constituted >65% of the total water supply, with irrigation accounting for ~70% of the total water usage. As a result, groundwater levels in the NCP declined at a rate of 1–2 m year<sup>-1</sup> by the end of the 20th century<sup>3,24</sup>, leading to an estimated cumulative depletion of ~60 km<sup>3</sup> from the 1960s to 2008<sup>25</sup>. In response to the acute water shortage in North China, the South-to-North Water Diversion (SNWD) project was initiated in 2002, diverting water from the humid Yangtze River basin. The high-quality diverted water has primarily been used to replace groundwater pumping for municipal and industrial purposes<sup>17,26</sup>. Additionally, excess diverted water has been used to replenish rivers and lakes and increase aquifer storage through MAR. Alongside strict groundwater pumping policies (e.g., shutting off wells and restricting groundwater pumping for irrigation when surface water is available), these measures have contributed to the stabilization and local recovery of groundwater levels in the NCP<sup>17,27</sup>. While conceptual and numerical models have indicated the potential for groundwater recovery across the NCP<sup>28,29</sup>, the actual extent of this

recovery has remained uncertain due to a lack of in-situ observations, which are often further hampered by spatiotemporal inconsistencies among monitoring well records.

In this study, we compiled and analyzed the most comprehensive dataset of in-situ groundwater level measurements to date across the NCP, from 2005 to 2024, with ~190,000 measurements from over 2000 wells. Our analysis reveals a significant recovery trend, with groundwater levels rising by ~0.7 m year<sup>-1</sup> on average across the NCP during 2020–2024. This recovery is primarily attributed to water diversions and active aquifer restoration policies. These findings challenge a previous study<sup>5</sup>, which may have underestimated the extent of groundwater recovery (Fig. 1f). Overall, our results provide critical insights into the potential for addressing groundwater depletion in cultivated drylands globally.

## Results

### Reversing groundwater depletion across the North China Plain

To investigate groundwater recovery in the NCP, we compiled an extensive dataset of in-situ groundwater level measurements from both unconfined and confined aquifers in urban and rural areas within the NCP. The establishment of China's national groundwater monitoring project in 2018 markedly improved the spatiotemporal coverage and quality of in situ measurements. Prior to 2018, there were many temporal discontinuities in the monitoring data, but the advent of an automatic monitoring system thereafter provided continuous data. Post-2018, there was a notable increase in monitoring well density in the NCP, particularly in the southeastern portions and in confined aquifers (Supplementary Fig. 1). For unconfined aquifers, groundwater levels were deepest (≥40 m) in the piedmont plain in the western portion of the NCP and shallowest (≤10 m) in the eastern portion of the NCP (Supplementary Fig. 1a–d). For confined aquifers, groundwater heads were deepest (≥70 m) in the cities of Tianjin, Cangzhou, and Hengshui (Supplementary Fig. 1e–h). Rapid shallowing trends have been observed across the NCP in both unconfined and confined aquifers (Fig. 2). We calculated Theil-Sen slopes for depth to groundwater at monitoring wells during 2020–2024 (Fig. 2m) because

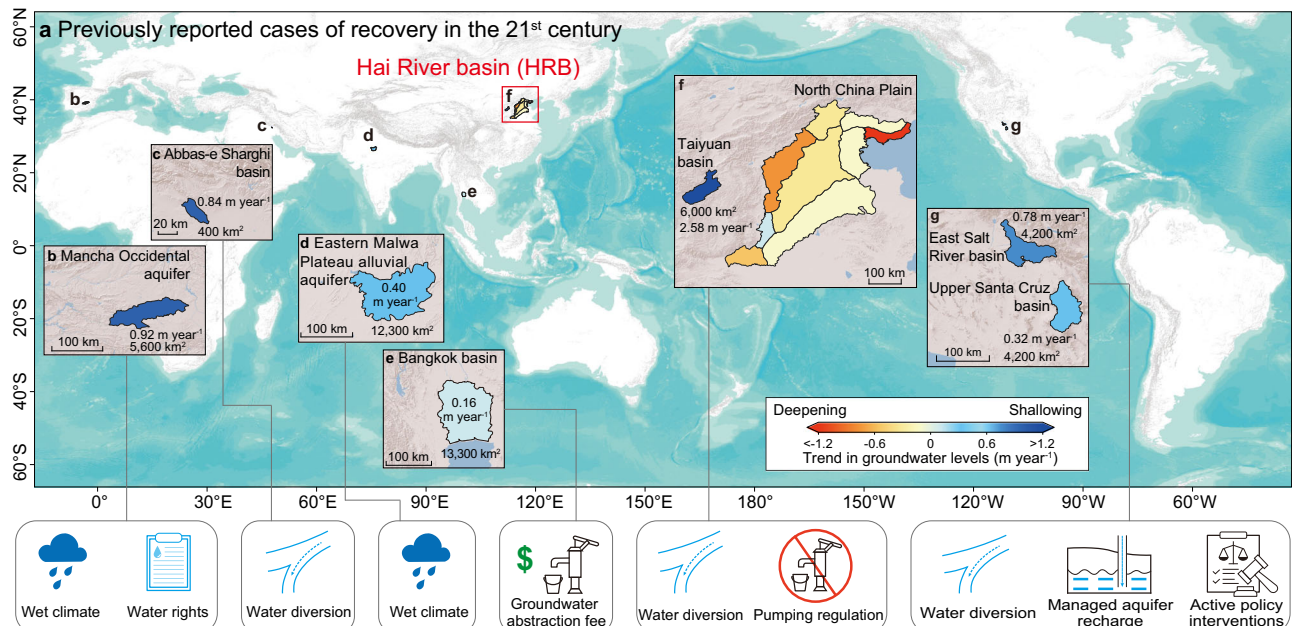


**Fig. 1 | Comparisons with previously reported cases of recovery.** **a** Previously reported groundwater recovery trends in the 21st century<sup>5</sup>, including the Mancha Occidental aquifer in Spain (**b**), Abbas-e Sharghi basin in Iran (**c**), Eastern Malwa Plateau alluvial aquifer in India (**d**), Bangkok basin in Thailand (**e**), Taiyuan basin in China (**f**), East Salt River and Upper Santa Cruz basins in the United States (**g**). The

trends previously reported for the North China Plain are also highlighted in (**f**)<sup>5</sup>. Positive trends (blue) indicate shallowing groundwater, while negative trends (red) indicate deepening groundwater. The main drivers for each recovery case<sup>13,14,18–21</sup> are also labeled.

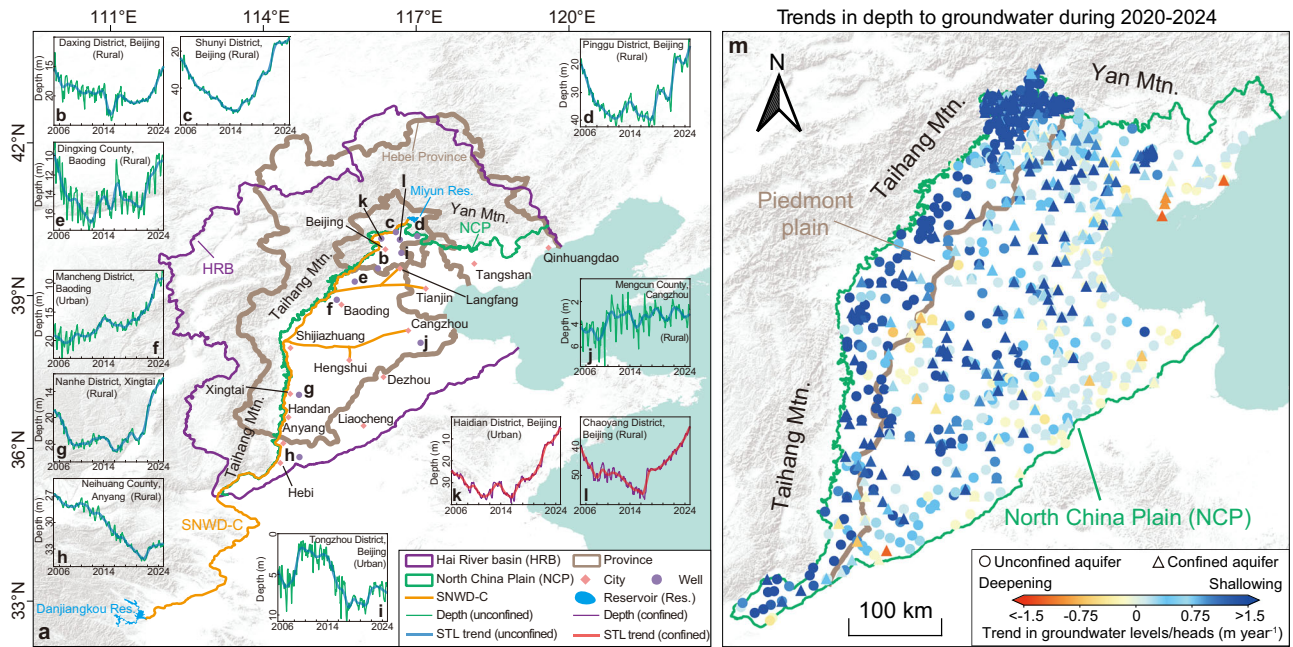


**Fig. 2 | Trends in groundwater depths across monitoring wells in the North China Plain and comparisons with previously reported cases of recovery.** **a** Overview of the Hai River basin (HRB). The purple line represents the boundary of the HRB. The green line represents the northern and western boundary of the North China Plain (NCP), which is the plain portion of the HRB. Orange lines represent the central route of the South-to-North Water Diversion (SNWD-C). Blue polygons represent reservoirs. Brown lines represent the boundaries of Hebei Province and the provincial-level municipalities of Beijing and Tianjin (Province). Red diamonds represent major cities. Purple circles represent the locations of monitoring wells (**b-l**). **b-j** Instances of continuous depth to groundwater measurements in

unconfined aquifers during 2005–2024. Green lines represent the depth to groundwater. Thick blue lines illustrate the long-term trends derived from STL decomposition. **k, l** Instances of continuous depth to groundwater measurements in confined aquifers during 2005–2024. Purple lines represent the depth to groundwater. Thick red lines illustrate the long-term trends derived from STL decomposition. **m** Trends in groundwater levels and heads at individual wells during 2020–2024. Circles indicate unconfined aquifers, while Deltas represent confined aquifers. Positive trends (blue) indicate shallowing groundwater, while negative trends (red) indicate deepening groundwater.

2020 marked the point of reversal in the average groundwater depth in the NCP. In unconfined aquifers, the most pronounced reversal in groundwater levels was found in the piedmont plain in the western portion of the NCP, with trends exceeding  $1.5 \text{ m year}^{-1}$  during 2020–2024. In confined aquifers, rapid shallowing trends in groundwater heads ( $\geq 1.5 \text{ m year}^{-1}$ ) were evident in the piedmont areas, as well as in the cities of Tianjin, Cangzhou, and Hengshui. Additionally, wells with continuous measurements indicated recovery in both urban and rural areas (Fig. 2b–l).

The groundwater level data indicate that the reversal of deepening trends in the average groundwater depth anomalies in both unconfined and confined aquifers occurred around 2020 (Fig. 3a). By the end of 2024, the average groundwater depth was  $-11 \text{ m}$  and  $-27 \text{ m}$  in unconfined and confined aquifers, respectively. In general, depths to groundwater in unconfined and confined aquifers are greatest in summer and smallest in winter, driven primarily by the combined effects of groundwater pumping for irrigation (peaking in spring) and recharge from precipitation (summer monsoonal rainfall accounting for  $\sim 60\%$  of annual precipitation). Seasonal variability in groundwater depth within a year is  $-1.5 \text{ m}$  in unconfined aquifers and  $-4 \text{ m}$  in confined aquifers. To mitigate the impact of seasonal variability, we isolated the long-term trends in the groundwater depth anomaly time series after removing the seasonal variability using STL decomposition. Our analysis shows that the rate of deepening in groundwater depth in unconfined aquifers slowed before the reversal in 2020 compared to the deepening trend in the late 20th century. Historically, groundwater levels in unconfined aquifers in the Piedmont Plain declined at a rate of  $1\text{--}2 \text{ m year}^{-1}$  during 1984–2005<sup>24</sup>. The deepening trend decreased to  $0.2 \text{ m year}^{-1}$  during 2005–2019, with relatively humid conditions in 2012 and 2016 contributing to mild recoveries. After the reversal in 2020, a rapid recovery rate of

$0.7 \text{ m year}^{-1}$  occurred during 2020–2024, with the average groundwater depth anomaly in unconfined aquifers in 2024 nearing levels last seen in 2005. For confined aquifers, we found a deepening trend of  $-0.5 \text{ m year}^{-1}$  during 2005–2019, followed by a recovery of  $-4 \text{ m}$  during 2020–2024. By 2024, the average groundwater head had returned to levels comparable to those in 2013. Notably, the recovery rates for both unconfined and confined aquifers decreased after 2021. Additionally, numerous sources have indicated a recovery in groundwater levels, as shown by the mitigation of land subsidence and re-emergence of springs in regions such as Beijing and Xingtai (see Methods).

Beijing experienced the first reversal of deepening groundwater levels in unconfined aquifers, followed by other cities in the NCP (Fig. 3b). Monitoring data from Beijing, the city with the highest quality data in the NCP, indicated the earliest reversal in 2016, followed by a recovery rate of  $1 \text{ m year}^{-1}$  during 2016–2024. Since 2021, Beijing’s groundwater level has been shallower than it was in 2005. In Baoding, the reversal occurred in 2020, with a recovery rate of  $1.5 \text{ m year}^{-1}$  during 2020–2024. By 2024, the groundwater level in Baoding was shallower than in 2005. The recovery of groundwater levels in Hengshui and Tangshan has been ongoing since 2021, albeit at a slower rate of  $0.4 \text{ m year}^{-1}$  and  $0.3 \text{ m year}^{-1}$ , respectively. The lower uncertainty in average groundwater depth anomalies for Beijing and the NCP, compared to Baoding, Hengshui, and Tangshan, underscores the importance of dense in-situ monitoring networks and comprehensive regional analysis in improving the reliability of groundwater assessments.

We identified and analyzed trends in groundwater depth at continuously monitored wells during 2005–2017 and 2018–2024 (Fig. 3c). A well displaying a monotonic deepening trend followed by a monotonic rebound was labelled as having a reversal of the

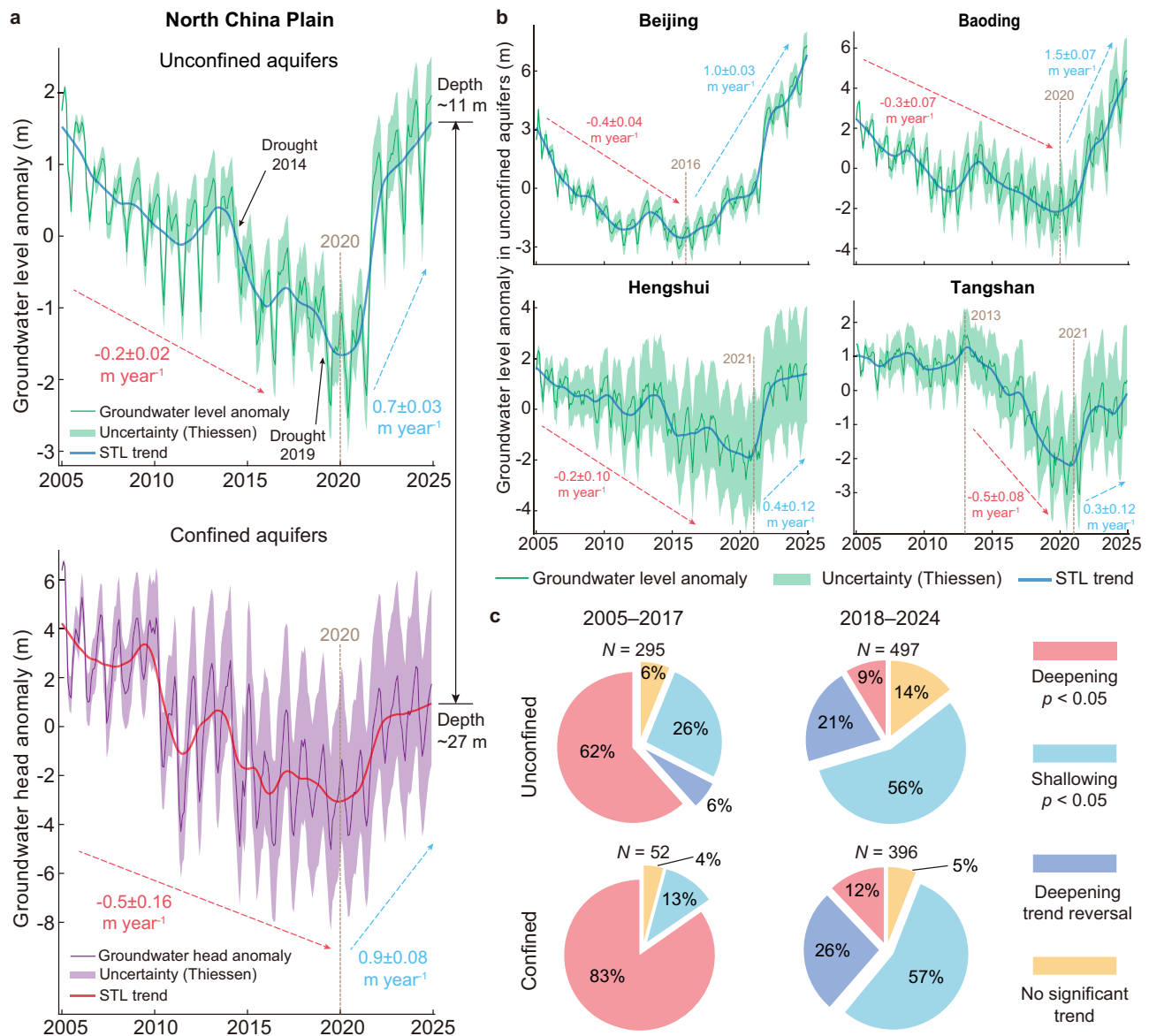


**Fig. 3 | Time series and trends in groundwater depths across the North China Plain.** **a** Time series of average groundwater level anomalies in unconfined and average groundwater head anomalies in confined aquifers. The green and purple lines represent the average groundwater level and head anomalies in unconfined and confined aquifers, respectively. The thick blue and red lines illustrate long-term trends in unconfined and confined aquifers derived from STL decomposition, respectively. The green and purple shadows represent the

uncertainty associated with the spatial distribution of the monitoring network and the application of the Thiessen polygon method in unconfined and confined aquifers, respectively. The dashed brown lines represent the timing of reversals. **b** Average groundwater level anomalies in unconfined aquifers at the city scale. Same legend as in (a). **c** Proportion of monitoring wells exhibiting deepening ( $p < 0.05$ , red), shallowing ( $p < 0.05$ , light blue), reversing ( $p < 0.05$ , dark blue), and no significant trend (orange) during 2005–2017 and 2018–2024.

deepening trend. For other wells, we assessed whether there was a significant deepening or shallowing trend ( $p < 0.05$ , MK test). Our findings show that significant deepening trends were predominant during 2005–2017, whereas significant shallowing trends became prevalent during 2018–2024. Approximately 62% and 83% of the monitoring wells in unconfined and confined aquifers show significant deepening trends during 2005–2017, respectively. Approximately 6% of the monitoring wells in unconfined aquifers, mainly in Beijing, experienced a reversal of the deepening trend during this period. In contrast, during 2018–2024, over half of the monitoring wells exhibited a significant shallowing trend, and about a quarter showed signs of a deepening trend reversal. These results align with the first reversal observed in Beijing in 2016 and the overall reversal at the NCP scale in 2020.

### Water supply and usage in the Hai River basin

The total water supply in the HRB has remained relatively stable from 2005 to 2023, averaging  $\sim 37$  km<sup>3</sup> annually, but the contribution of different water sources has shifted significantly (Fig. 4a, b). In 2005, groundwater accounted for about two-thirds of the total water supply, with unconfined aquifers providing 18.7 km<sup>3</sup>, nearly three times the 6.6 km<sup>3</sup> supplied by confined aquifers. Around 2009, groundwater extraction from confined aquifers began to decline, providing 5% less in 2014 relative to the volume provided in 2005, with reclaimed water compensating for most of this reduction. Meanwhile, surface water supply from reservoirs increased (+1.8 km<sup>3</sup>) during 2005–2023 and now constitutes over a quarter of the total water supply. Water diverted from the Yellow River remained stable at  $-4.4$  km<sup>3</sup> annually, representing 10% of the total water supply, except for a spike in 2019

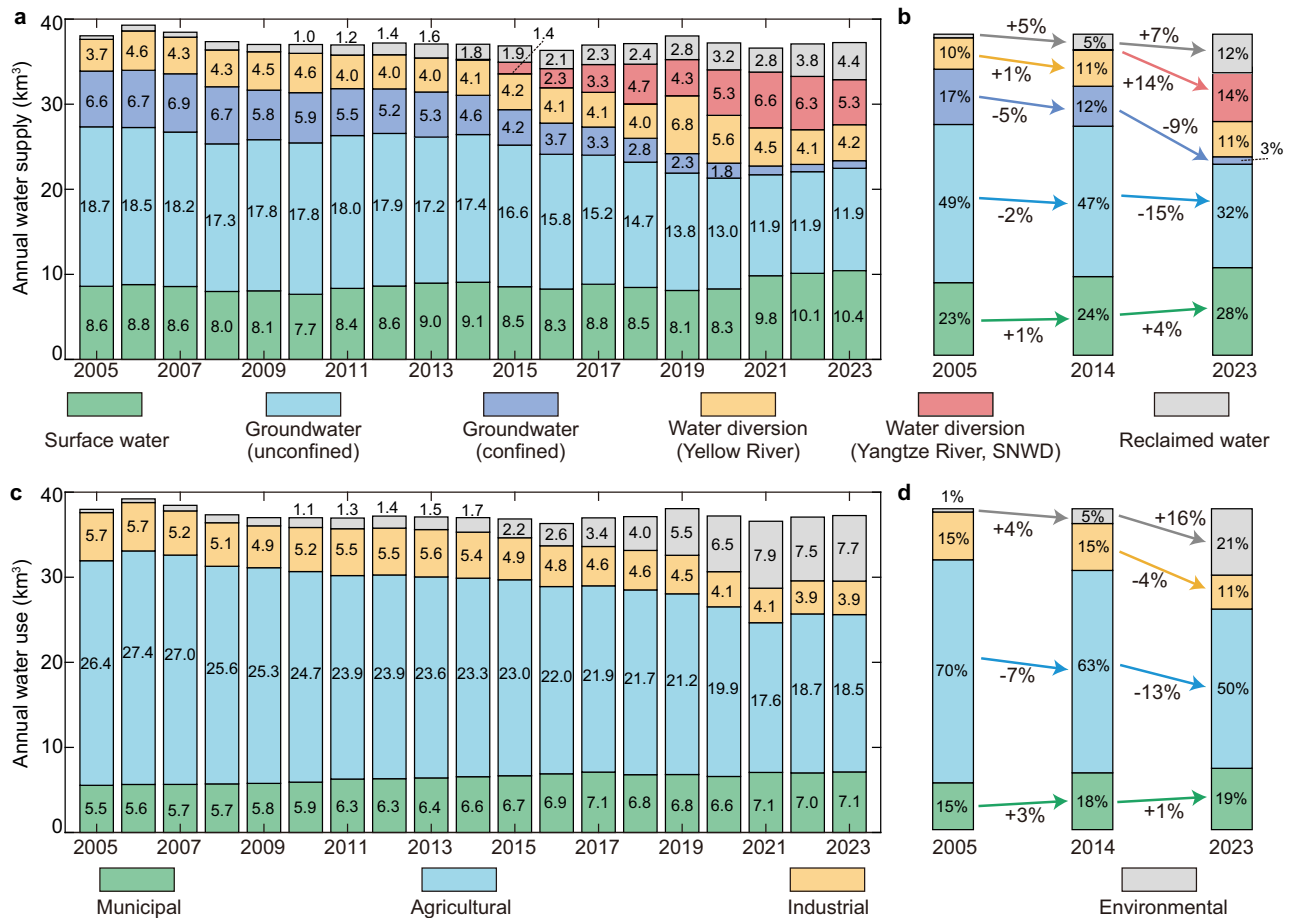


**Fig. 4 | Annual water supply and usage in the Hai River basin. a** Annual water supply from various sources (km<sup>3</sup>), including surface water from reservoirs, groundwater from unconfined and confined aquifers, water diversion from the Yellow River, water diversion from the Yangtze River (South-to-North Water

Diversion, SNWD), and reclaimed water. **b** Proportions of total water supply in 2005, 2014, and 2023. **c** Annual water use across different sectors (km<sup>3</sup>), including municipal, agricultural, industrial, and environmental water usage. **d** Proportions of total water use in 2005, 2014, and 2023.

and 2020. Reclaimed water use grew steadily, reaching 4.4 km<sup>3</sup> by 2023 and accounting for 12% of the total water supply in 2023. Reclaimed water is primarily used for river and lake replenishment, as well as for sanitation, landscape irrigation, and industry. Despite initiatives promoting desalination, the use of desalinated seawater in the HRB has remained minimal, with an annual capacity of -0.25 km<sup>3</sup> in 2023, contributing <1% to the total water supply.

The central route of the South-to-North Water Diversion (SNWD-C), which began operations in December 2014, introduced significant diversification into the water supply structure of the HRB. The SNWD-C was designed to divert 9.5 km<sup>3</sup> of high-quality water annually from the Danjiangkou Reservoir on the Han River, the largest tributary of the Yangtze River, to northern China. The eastern route of the SNWD (SNWD-E), which diverts water from Jiangdu near the Yangtze River, supplies a small amount of water (-0.2 km<sup>3</sup> year<sup>-1</sup>) to the southeastern parts of the NCP, with the majority benefiting areas in Shandong Province outside the NCP. In 2023, the SNWD provided 5.3 km<sup>3</sup> of water, accounting for 14% of the total supply, making it the third largest source after unconfined aquifers (11.9 km<sup>3</sup>, 32%) and surface water from reservoirs (10.4 km<sup>3</sup>, 28%).

Groundwater usage in 2023 (-13 km<sup>3</sup>) was nearly half of what it was in 2005 (-25 km<sup>3</sup>), with a steeper decline in confined aquifers (-85% reduction) than in unconfined aquifers (-36% reduction) from 2005 to 2023. By 2023, pumping from confined aquifers decreased to <1 km<sup>3</sup>, accounting for only 3% of the total water supply. This greater reduction in confined aquifer use is largely attributed to its greater substitution

by water from the SNWD project. Historically, confined aquifers, valued for their high water quality, have been a primary source for municipal use, particularly because unconfined aquifers are more vulnerable to contamination. With the introduction of water from the SNWD project, groundwater from confined aquifers that had been used for municipal supplies has increasingly been replaced, thereby reducing groundwater pumping. However, the SNWD supply is affected by drought conditions in its source areas. For example, drought conditions upstream of the Danjiangkou Reservoir led to the SNWD supply being decreased by 16% from 2022 to 2023 (from 6.3 km<sup>3</sup> to 5.3 km<sup>3</sup>).

Despite generally stable total water use, a shift towards increased allocation to environmental flows has led to a reduction in total municipal, agricultural, and industrial use, from 37.6 km<sup>3</sup> in 2005 to 29.5 km<sup>3</sup> in 2023 (Fig. 4c, d). Agricultural water use, which accounted for 70% of the total in 2005, has steadily declined to 50% by 2023. In addition to a -10% decrease in cropland area (Supplementary Fig. 2), this reduction is attributed to policies aimed at mitigating water shortages and curbing groundwater extraction, including adjustments to cultivation practices, dryland farming, seasonal fallow, and use of plastic mulch to conserve soil moisture<sup>30</sup>. Municipal water use increased by -30% during 2005–2023, driven by population growth, while industrial water use decreased by a similar percentage due to conservation efforts<sup>31</sup>. Environmental water use, which includes watering trees and grasslands as well as replenishing lakes and rivers<sup>17</sup>, has been over 7 km<sup>3</sup> since 2021, becoming the second-largest water use

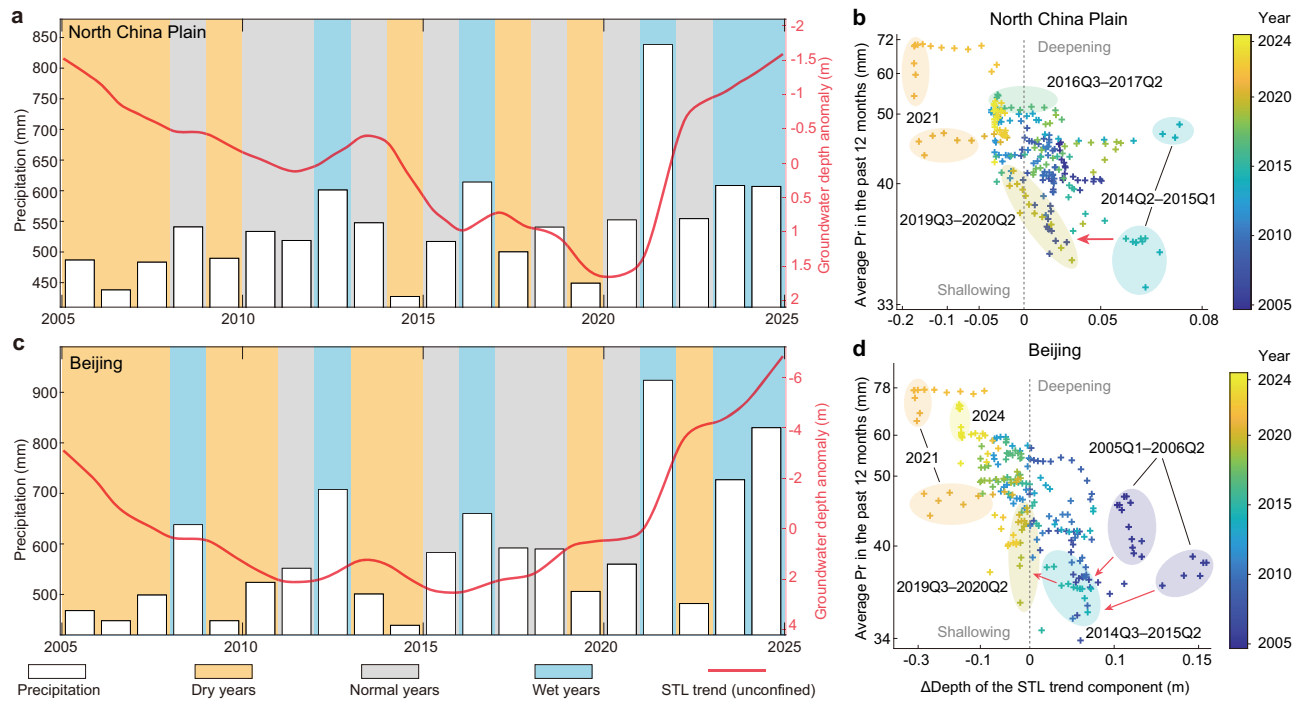


**Fig. 5 | Groundwater depth response in unconfined aquifers to precipitation variability.** **a** Annual precipitation in the Hai River basin (HRB, white bars) and average groundwater depth anomalies in unconfined aquifers across the North China Plain (NCP). Background shading denotes dry (orange), normal (gray), and wet (blue) years. The red line shows the long-term trend in average groundwater depth anomalies, derived via STL decomposition. **b** Scatter plot relating 12-month average precipitation (Pr) in the HRB to the corresponding change in the STL trend

component of groundwater depth anomalies in the NCP. Both axes use logarithmic scales. Point colors indicate months, and labels such as “2014Q2” denote the year and calendar quarter. The red arrow indicates the leftward shifts observed during droughts. The dashed gray line indicates a stable trend. **c** Same as (a), but for Beijing: annual precipitation and groundwater depth anomalies in unconfined aquifers. **d** Same as (b), but for Beijing: precipitation-groundwater trend relationships based on STL decomposition.

sector (>20% of the total) after agriculture. Reclaimed water, along with water diverted from the Yellow and Yangtze rivers and surface water from reservoirs<sup>32</sup>, plays a crucial role in supporting these environmental flows<sup>17</sup>.

### Water diversion and aquifer restoration policies drive groundwater recovery

The observed groundwater recovery in the NCP is primarily attributable to sustained human intervention, with wet years (e.g., 2021) providing additional but temporary reinforcement (Fig. 5). A pivotal measure was the substitution of groundwater pumping with water from SNWD-C. Initially, in 2015, Beijing received the bulk of diverted water (0.8 km<sup>3</sup> out of 1.4 km<sup>3</sup> delivered to the NCP), which led to an early recovery of groundwater levels beginning in 2016. This recovery remained resilient even during droughts in 2019 and 2022 (Fig. 5c). After 2020, SNWD-C deliveries expanded to other parts of the NCP, reaching over 4 km<sup>3</sup> per year and supporting a broader reversal of regional groundwater declines (Fig. 5a).

The coupling between precipitation and groundwater depth anomalies further highlights the impact of these interventions (Fig. 5b, d). A systematic leftward shift in precipitation-groundwater scatter plots indicates increasingly shallow groundwater conditions, even under similar rainfall conditions. These shifts are particularly pronounced during drought years (the red arrow in Fig. 5b), suggesting that the interventions have altered the groundwater balance and strengthened the system’s resilience. A similar pattern is observed in Beijing (Fig. 5d), where 2024 groundwater depths significantly improved compared to 2005. Although the extreme rainfall in 2021 temporarily accelerated groundwater recovery, its effect was short-lived, as soil moisture returned to baseline levels by early 2022 (Supplementary Fig. 3). In contrast, the continued groundwater rises

in Beijing (2016–2020) and the ongoing NCP-wide recovery since 2022 underscore the effectiveness and durability of policy-led groundwater restoration efforts.

MAR and reduced irrigation-related pumping are critical strategies for restoring depleted aquifers (Fig. 6a–c). For years, rivers in the NCP had dried up due to upstream reservoir interception and declining groundwater levels. Experimental river replenishment began in 2018 in the Fuyang, Hutuo, and Juma rivers. Since then, over 10 km<sup>3</sup> of water from the SNWD project has been allocated to restore rivers across the NCP by 2024. Additional contributions came from Yellow River diversions and local reservoirs, benefiting rivers (e.g., the Yongding River) and lakes (e.g., the Baiyangdian Lake). These efforts have rejuvenated drying rivers, restored riparian ecosystems, and enhanced aquifer recharge. Wells near replenished rivers exhibited more rapid groundwater recovery rates (Fig. 6b), confirming the effectiveness of river-based MAR. Other MAR methods, including flood-restoring recharge ponds and injection wells targeting confined aquifers, were employed but at smaller scales. In parallel, changes in irrigation practices also contributed to partial recovery. The NCP’s dominant double cropping system (winter wheat and summer maize rotation) requires intensive spring irrigation, historically sustained by groundwater pumping. Between 2013 and 2018, the area under double cropping declined by -10,000 km<sup>2</sup><sup>30</sup>. In rural areas between Beijing and Langfang, where the reduction was the greatest<sup>30</sup>, groundwater recovery began as early as 2013–2014 (Fig. 6c). Since 2018, further decline in double-cropped area has slowed, as diverted water has allowed local surface water to be redirected for irrigation<sup>30</sup>. In contrast, the southeastern NCP retained stable cropping patterns due to reliance on Yellow River diversions. Despite the cropping adjustments, regional food production in Beijing, Tianjin, and Hebei rose from -28 million tons in 2005 to -42 million tons in 2023 (Supplementary

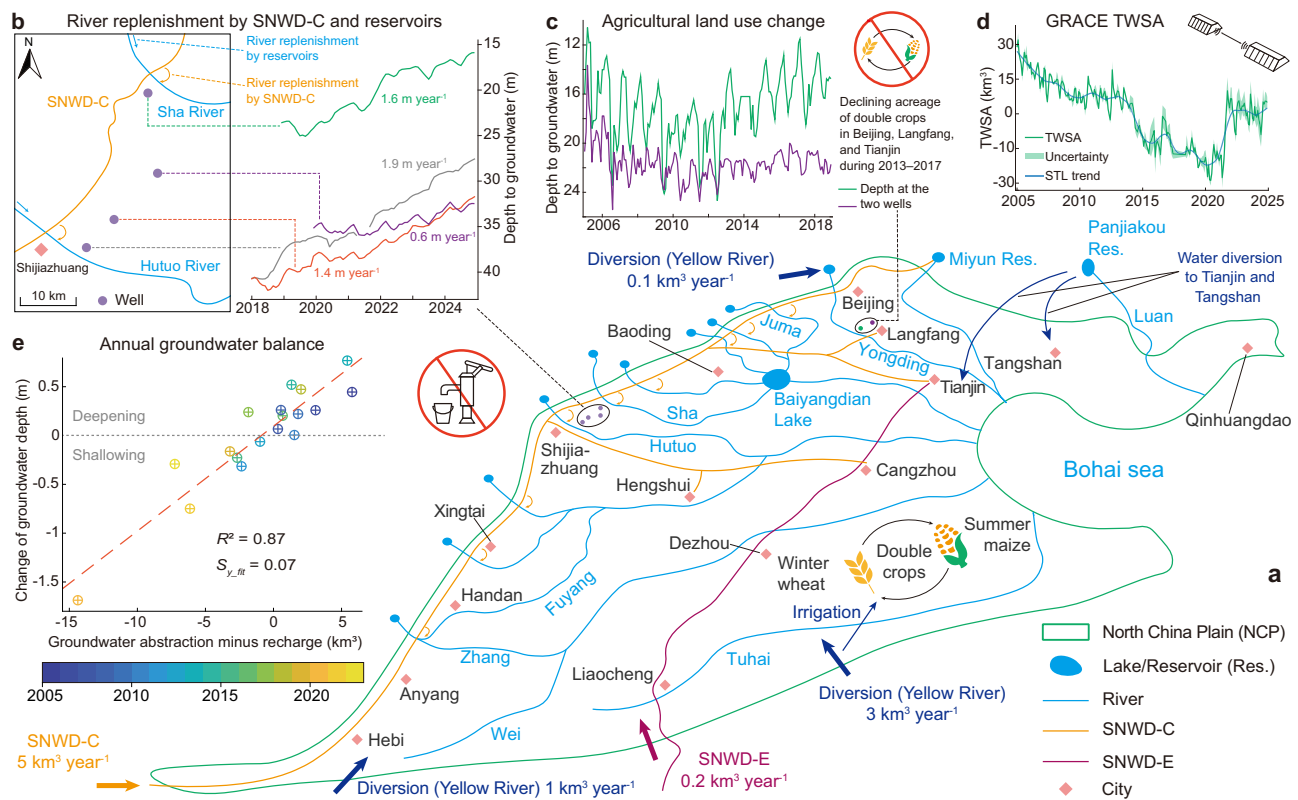


**Fig. 6 | Engineering and policy approaches for reversing groundwater depletion.**

**a** Water diversion and river replenishment in the North China Plain (NCP). The green line represents the boundary of the NCP. Blue polygons represent lakes and reservoirs. Blue, orange, and dark red lines represent rivers, the central route of the South-to-North Water Diversion (SNWD-C), and the eastern route of the South-to-North Water Diversion (SNWD-E), respectively. **b** Groundwater depth in unconfined aquifers near replenished rivers. Green, purple, gray, and red lines correspond to four monitoring wells located between the Sha and the Hutuo rivers from 2018 to 2024. **c** Groundwater depth in unconfined aquifers in areas where double-cropped acreage declined substantially between 2013 and 2017. Green and purple lines

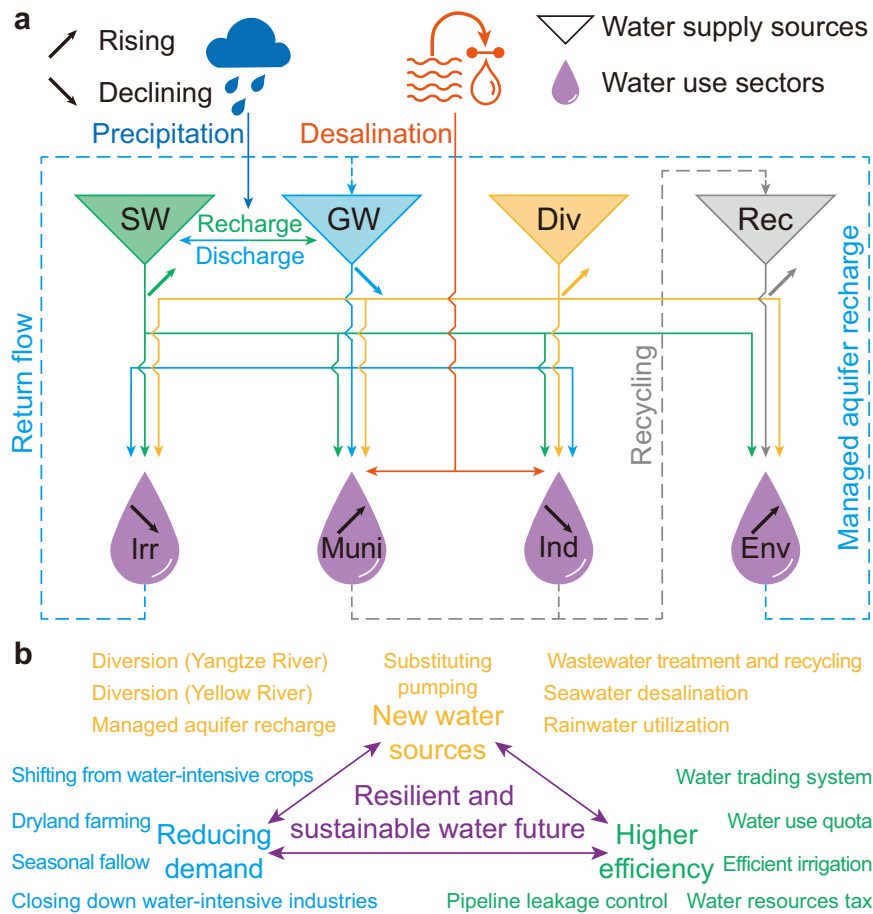
represent two representative monitoring wells. **d** GRACE-derived total water storage anomalies (TWSA) in the NCP. The green line shows the average of the JPL and CSR mascon products; the shaded green area shows their spread. The thick blue line represents the trend (based on STL decomposition). **e** Annual groundwater balance in the NCP from 2005 to 2023. The x axis shows net groundwater abstraction (abstraction minus recharge) based on Hai River Water Resources Bulletins ( $\text{km}^3$ ). The y axis represents the annual change in the trend in groundwater depth (based on STL decomposition) in unconfined aquifers, with the dashed gray line indicating a stable trend.  $S_{y,fit}$  indicates the fitted specific yield derived from the slope of the balance-depth relationship.

Fig. 4)<sup>33</sup>, aided by increased yield per unit area, helping to ensure local food security.

Groundwater depth recovery observed in monitoring wells is consistent with both satellite-based and water balance estimates (Fig. 6d, e). Interannual changes in groundwater depth in unconfined aquifers show a strong linear relationship ( $R^2 = 0.87$ ) with net water balance deficits, calculated as annual groundwater abstraction minus recharge from the Hai River Water Resources Bulletins (Fig. 6e). The fitted specific yield ( $S_{y,fit}$ ) of 0.07 generally matches reported values of  $-0.12$  in the piedmont plains and  $-0.04$  in other regions of the NCP<sup>25</sup>, supporting the reliability of the water balance approach<sup>34</sup> (see Methods). Satellite observations from GRACE and GRACE-FO show a recovery in total water storage anomalies (TWSA) beginning around 2020 (Fig. 6d), yet this rebound compensates for only about half of the  $-49 \text{ km}^3$  of total water storage depletion between 2005 and 2019. Based on a 3 m decline in groundwater level and the estimated  $S_{y,fit}$ , unconfined aquifer storage alone decreased by  $-27 \text{ km}^3$  during this period. Confined aquifers, characterized by much smaller storage coefficients (0.0004–0.004), contributed relatively little to the total depletion, indicating that the majority of groundwater loss occurred in unconfined systems<sup>25</sup>. Discrepancies between GRACE TWSA data and in-situ groundwater trends likely stem from variations in soil and surface water storage, uncertainties in specific yield and storage coefficients, or inherent limitations in GRACE resolution. A full attribution of these differences is beyond the scope of this study.

## Discussion

Human intervention has successfully reversed groundwater depletion in the NCP through a combination of new water sources, reduced water demand, and enhanced water use efficiency with strict groundwater pumping regulations (Fig. 7). Key strategies included water diversion and wastewater recycling, which diversified the water supply and reduced reliance on overexploited aquifers. Excess water has been utilized for replenishing water bodies and MAR, contributing to aquifer restoration and enhancing system resilience against future droughts. To reduce agricultural water demand, several approaches were implemented, including shifting from water-intensive crops (e.g., transitioning from wheat-maize rotations to single maize crops that coincide with the summer rainy season<sup>30</sup>), expanding dryland farming, and introducing seasonal fallow periods. Additionally, water-intensive industries (e.g., steel and papermaking plants) were phased out. Engineering solutions, such as water-saving irrigation systems and pipeline leakage control, further improved water use efficiency. Effective management tools, such as water resources taxes, water use quotas (e.g., annual water use quotas for Beijing ( $4.25 \text{ km}^3$ ), Tianjin ( $3.5 \text{ km}^3$ ), and Hebei ( $20.6 \text{ km}^3$ )), and water trading systems, were also introduced to optimize scarce water resources, stimulating more efficient usage<sup>35</sup>. As a result, water productivity in the NCP has increased three to four times between 2005 and 2023. In 2023, economic output per unit of water use reached  $-\$50 \text{ m}^{-3}$  based on gross domestic product (GDP) and  $-\$120 \text{ m}^{-3}$  based on industrial added



**Fig. 7 | Water supply and use amid human intervention in the Hai River basin.** **a** Schematic diagram of water supply and use, with Deltas representing major water sources: surface water (SW), groundwater (GW), diverted water (Div, including the South-to-North Water Diversion and diversion from the Yellow River), and reclaimed water (Rec). Purple droplets indicate water use sectors: irrigation (Irr), municipal use (Muni), industry (Ind), and environmental use (Env). Solid lines link

water sources and water use sectors, while dashed lines represent potential ways for used water to be returned as resources. Arrows depict rising and declining trends over the past two decades. **b** Policy and engineering approaches applied: yellow, blue, and green indicate approaches related to new water sources, reducing water demand, and improving water use efficiency, respectively.

value, compared to just  $-\$17\text{ m}^{-3}$  and  $-\$27\text{ m}^{-3}$ , respectively, in 2005 (all values adjusted to 2023 constant prices)<sup>36</sup>. Annual irrigation intensity decreased by more than 30% from 2005 ( $0.37\text{ m}^3\text{ m}^{-2}$ ) to 2023 ( $0.24\text{ m}^3\text{ m}^{-2}$ ). Together with stringent pumping regulations (e.g., closure of >27,000 wells by 2023 according to the Ministry of Water Resources), these activities effectively curbed the potential for the Jevons Paradox, where increased efficiency could have led to higher overall water consumption<sup>37</sup>. This successful recovery offers valuable insights for restoring depleted aquifers in other global hotspots facing similar challenges, including regions in Iran<sup>38</sup>, Iraq<sup>39</sup>, Turkey<sup>40</sup>, Lebanon<sup>41</sup>, Jordan<sup>42</sup>, central South Africa<sup>43</sup>, California’s Central Valley<sup>44,45</sup> and the Southern and Central High Plains<sup>45,46</sup> of the United States, and the Indo-Gangetic Plain<sup>47</sup>.

Water diversion has played a pivotal, though not exclusive, role in alleviating water scarcity and restoring overexploited aquifers, particularly in densely populated semi-humid to semiarid regions with extensive irrigation. Projects such as the SNWD, Central Arizona Project<sup>12</sup>, California’s water-delivery system (Central Valley Project and State Water Project)<sup>48</sup>, and the water diversion from the Sea of Galilee in Israel<sup>49</sup> have substituted for local aquifer pumping, contributing to groundwater storage recovery. Additionally, water diversions in eastern South Africa and the Toshka District of Egypt<sup>50</sup>, though not primarily intended for aquifer restoration, have also helped reduce pumping in these rapidly developing areas vulnerable to groundwater depletion<sup>43</sup>. However, even with these water diversion projects,

challenges remain. For instance, despite efforts in California’s Central Valley to mitigate water deficits<sup>15</sup>, wells have run dry during recent droughts<sup>44</sup>. Although vast irrigation canals increased groundwater storage through increased recharge in the early 20th century<sup>51</sup>, increased irrigation from India’s river interlinking project could reduce rainfall in September in already water-stressed regions due to land-atmosphere feedback<sup>52</sup> and lead to increased groundwater pumping. These cases underscore the need to control water demand even when additional diverted water is available.

Policy and engineering solutions must work in tandem to tackle groundwater depletion. Measures similar to those implemented in the NCP, such as diverting water from the Colorado River, enforcing pumping regulations, limiting irrigation water use, and increasing the use of reclaimed water, have been applied in Arizona’s active management areas (AMAs), leading to successful groundwater storage recovery<sup>12,53,54</sup>. The reversal of groundwater level declines in Israel’s coastal plain aquifer during the late 1960s also benefited from water diversion, wastewater reclamation, and reduction of pumping<sup>49</sup>. MAR, the process of artificially recharging water into the subsurface, supports the conjunctive use of surface water and groundwater, increasing system resilience to climate extremes<sup>1</sup>. MAR has contributed to reversing groundwater depletion trends in the NCP, California’s Central Valley, and Arizona’s AMAs<sup>18</sup>, with further potential applications in India<sup>55</sup>, Africa<sup>56</sup>, and Europe<sup>57</sup>. Desalination faces challenges, such as managing brine waste<sup>58</sup> and higher costs compared to wastewater

recycling<sup>59</sup>, limiting its application<sup>1</sup>. However, wastewater recycling, as demonstrated in the NCP and Arizona’s AMAs<sup>12</sup>, could significantly alleviate water scarcity with the added co-benefit of improved water quality. Our results demonstrate that rapid groundwater recovery across a vast area (NCP: -130,000 km<sup>2</sup>) is feasible through water diversions and policy interventions, offering a valuable example for water resource managers globally.

## Methods

### Groundwater level data collection

The reform of China’s groundwater monitoring system around 2018 led to a discontinuity in the availability of depth to groundwater data for the NCP, with most studies only including data before 2019<sup>5,26–28</sup> or after 2017<sup>60</sup>. Since 2005, the China Institute for Geo-Environment Monitoring published the Yearbooks of Groundwater Levels, providing the first publicly available and most comprehensive dataset of groundwater depth across China. However, before the establishment of the national groundwater monitoring project in 2018, monitoring wells were sparse, data quality was inconsistent, and only a limited number of wells provided continuous data, with observation intervals varying from daily to monthly. Since 2018, newly installed monitoring wells have automatically recorded groundwater depth at 1–4 hour intervals, resulting in continuous time series data and improving the reliability of monthly averages used in this study. Monthly average groundwater depth data for 2005–2017 were digitized from the printed Yearbooks of Groundwater Levels, while data from 2018 to 2024 were obtained from the China Institute for Geo-Environment Monitoring’s online platform (<https://geocloud.cgs.gov.cn>).

### Data preprocessing

Quality control and interpolation procedures were applied before aggregating groundwater depth data at regional scales. Three parameters were defined for preprocessing: (1) maximum allowable gap for linear interpolation (*intrplGap* = 3 months), (2) minimum length of time series required (*minLen* = 48 months), and (3) moving window size for outlier detection (*windowOL* = 24 months). First, linear interpolation was applied to internal data gaps not exceeding *intrplGap*. Second, wells with fewer than *minLen* months of valid observations were excluded from the analysis. Third, a moving average filter with a window length of *windowOL* months was used to identify and mask outliers, defined as values deviating by more than three standard deviations from the moving average. These thresholds were selected based on data characteristics and preliminary sensitivity analyses to ensure robust spatiotemporal coverage while minimizing the influence of outliers.

### Analyses of depth to groundwater in the NCP

The Quaternary aquifers in the NCP are typically divided into four aquifers, with the shallowest being unconfined and the remaining three confined<sup>25</sup>. In the piedmont plain, water is primarily pumped from the unconfined aquifer, whereas in other regions, it mainly comes from the confined aquifers because of the presence of saline and brackish water in the unconfined aquifer<sup>24,61</sup>.

We aimed to develop a consistent understanding of groundwater depth dynamics across various regional scales over the past two decades, particularly under the reformed groundwater monitoring system around 2018. First, we calculated the change in groundwater depth between consecutive months and applied a weighted average to the groundwater depth changes at each available monitoring well, using the corresponding areas of Thiessen polygons as the basis for weighting:

$$\overline{\Delta Dph_j} = \frac{\sum_i S_i \times (Dph_{i,j} - Dph_{i,j-1})}{S_{tot}} \quad (1)$$

where *Dph<sub>i,j</sub>* and *Dph<sub>i,j-1</sub>* represent the groundwater depth in months *j* and *j-1* at each monitoring well, *S<sub>i</sub>* is the area of the Thiessen polygon associated with the well, and *S<sub>tot</sub>* is the area of the target region (each well was associated with a unique polygon). This equation means that only wells with valid groundwater depth measurements in both months *j* and *j-1* were included in the spatial averaging. Second, we summed the changes to obtain the cumulative change:

$$\Delta Dph_{cum_i} = \sum_{j=1}^i \overline{\Delta Dph_j} \quad (2)$$

Groundwater depth anomalies were then calculated as anomalies of the cumulative change (*ΔDph<sub>cum<sub>i</sub></sub>*). Finally, we employed the Seasonal and Trend decomposition using Loess (STL) to decompose the average depth series into trend, seasonal, and remainder components. The Theil-Sen slope<sup>62,63</sup> was used to assess the trends in the STL components because it is robust against outliers and effective for analyzing trends in groundwater depth<sup>5</sup>.

Our results show that the selection of preprocessing parameters minimally impacted the main findings (Supplementary Fig. 5a, b). To assess the uncertainty introduced, we tested a range of values: *intrplGap* from 1 to 5, and *minLen* and *windowOL* of 12, 24, 36, 48, and 60, ensuring that *windowOL* did not exceed *minLen*. Although aggregating monthly changes in groundwater depth introduced some uncertainty, the influence of preprocessing selections remained limited, as indicated by the shaded areas in Supplementary Fig. 5a, b. The number of monitoring wells available increased significantly after 2018 (Supplementary Fig. 5c). For unconfined aquifers, well coverage rose from -400 to -500 in 2010 to -500 to -700 in 2018. For confined aquifers, the number increased from -120 wells before 2018 to -700 after 2018. We analyzed changes in groundwater depth rather than absolute levels, which reduced the sensitivity of regional trends to data gaps or inconsistencies in well continuity. Groundwater heads in different confined aquifer layers followed two general patterns (Supplementary Fig. 5d). First, deeper layers typically had greater depths to groundwater. Second, due to intensive pumping and vertical leakage through aquitards, groundwater heads across layers were often similar. We did not analyze the dynamics of groundwater heads across different confined layers at the regional scale, primarily due to the limited number of monitoring wells in the second and third confined layers, particularly before 2018.

We assessed the uncertainty associated with the spatial distribution of the monitoring network and the application of the Thiessen polygon method using Monte Carlo simulations. In each of the 10,000 simulations, 95% of available monitoring wells were randomly selected to calculate the monthly average groundwater depth. This approach accounts for the -5% month-to-month fluctuation in well availability.

From the simulation results *D*, we computed the 90% confidence interval (CI) and standard deviation (*σ*) as follows:

$$CI = [D_{5\%}, D_{95\%}] \quad (3)$$

$$\sigma = \sqrt{Var(D)} \quad (4)$$

where *D<sub>5%</sub>* and *D<sub>95%</sub>* represent the 5th and 95th percentiles of the simulation ensemble.

Trend significance was evaluated using the Mann–Kendall test at a significance level of *p* < 0.05 (two-tailed)<sup>64</sup>. For individual wells (Fig. 2b–l), trends were estimated using the Theil-Sen slope applied to raw time series data to accommodate data discontinuities. At the city scale (Fig. 3b), we selected four cities, Beijing, Baoding, Hengshui, and Tangshan based on data availability sufficient to generate continuous time series before and after 2018. For trend classification at the well level (Fig. 3c), we considered only wells with complete data for both

the 2005–2017 and 2018–2024 periods. A “reversal” of the groundwater deepening trend was identified only when a monotonic decline was followed by a monotonic rebound. Wells with non-monotonic recovery patterns were categorized as “shallowing”.

### Statistic data of water resources

We compiled data on precipitation, renewable groundwater resources, water productivity, and water supply and use from the Hai River Water Resources Bulletins (<http://www.hwcc.gov.cn/wwgj/xxgb/szygb/>) and the China Water Resources Bulletins (<http://mwr.gov.cn/sj/tjgb/szygb/>). The data include detailed breakdowns of water sources, except for certain years where some information was missing. For example, the breakdown of diverted water in 2016 and 2017 was interpolated based on data from adjacent years, considering the relatively stable water diversion from the Yellow River. Regional data were collected from the Water Resources Bulletins of Beijing (<https://swj.beijing.gov.cn/zwgk/szygb/index.html>), Tianjin ([https://swj.tj.gov.cn/zwgk\\_17147/xzfxgk/fdzdgknr1/tjxx/](https://swj.tj.gov.cn/zwgk_17147/xzfxgk/fdzdgknr1/tjxx/)), Hebei (<http://slt.hebei.gov.cn/a/zfxgk/>), and Shandong ([http://wr.shandong.gov.cn/zwgk\\_319/fdzdgknr/tjsj/szygb/](http://wr.shandong.gov.cn/zwgk_319/fdzdgknr/tjsj/szygb/)). Economic output values of water use were adjusted to 2023 constant prices using GDP deflator data from the World Bank (<https://data.worldbank.org/indicator>) and Producer Price Index (PPI) data from the National Bureau of Statistics of China (<https://www.stats.gov.cn/sj/>). Additionally, desalination capacity data were obtained from the National Seawater Use Bulletin (<https://www.mnr.gov.cn/sj/sjfw/>).

### Relationship between precipitation and changes in groundwater depth

We analyzed the relationship between precipitation and changes in groundwater depth to assess the impact of human intervention on groundwater recovery. To present precipitation (vertical axes of Fig. 5b, d), we used the 12-month moving average, as its influence on aquifer recharge can be long-lasting:

$$Pr_{Avg12}(t) = \frac{\sum_{i=t-11}^t Pr(i)}{12} \quad (5)$$

where  $Pr_{Avg12}(t)$  is the 12-month moving average precipitation for month  $t$ , and  $Pr(i)$  is the precipitation in month  $i$ .

To represent changes in groundwater depth (horizontal axes in Fig. 5b, d), we used the month-to-month difference in the trend component of aggregated groundwater depth anomalies:

$$\Delta Dph_{trend}(t) = Dph_{trend}(t) - Dph_{trend}(t-1) \quad (6)$$

where  $\Delta Dph_{trend}(t)$  is the change in the STL trend component of groundwater depth anomalies for month  $t$ , and  $Dph_{trend}(t)$  is the STL trend component itself for month  $t$ .

### Estimation of average specific yield

The average specific yield in the NCP was estimated with a water balance method<sup>34</sup> that uses the relationship between changes in groundwater depth within unconfined aquifers and groundwater abstraction minus recharge. The following equation was applied:

$$\Delta Dph = \frac{Pumping - Recharge}{S_{y,fit} \times Area_{NCP}} + C \quad (7)$$

where  $\Delta Dph$  is the annual groundwater depth change in unconfined aquifers,  $S_{y,fit}$  is the fitted specific yield,  $Area_{NCP}$  is the area of the NCP, and  $C$  is a constant.

### Other evidence of groundwater recovery

In addition to the recovery in groundwater depth, land subsidence in the NCP has also stabilized or begun to recover. Land subsidence in the

NCP has worsened since the 1950s<sup>65</sup>, but there have been instances of stabilization and recovery in Beijing<sup>66</sup>, Tianjin<sup>66</sup>, and Cangzhou<sup>67</sup>. Springs have re-emerged in Mentougou in Beijing ([https://www.beijing.gov.cn/renwen/jrbj/202304/t20230419\\_3059190.html](https://www.beijing.gov.cn/renwen/jrbj/202304/t20230419_3059190.html)), and in Bai Springs in Xingtai (<http://slt.hebei.gov.cn/a/2022/07/22/7BACE2B982F842A387544296E12E9AOF.html>). The thickening of the unsaturated zone due to depletion has likely significantly reduced recharge<sup>68</sup>, so a recovery in groundwater levels could potentially lead to increased recharge.

### Limitations

Despite using the best available in situ groundwater depth data for the NCP, several limitations remain. First, continuous observations were available for only a limited number of wells, particularly prior to 2018. Data before 2017 were often irregular, with varying measurement frequencies and sparse spatial coverage, particularly in the southeastern NCP. These limitations in groundwater monitoring introduce uncertainty when applying spatial interpolation using the Thiessen polygon method. In areas with sparse data, wells receive disproportionately high weights, which may affect the representativeness and reliability of regional estimates. Second, more rapid recovery observed in urban areas compared to rural regions, largely driven by the replacement of municipal groundwater pumping with water from the SNWD project, could introduce bias when well distribution is uneven. To minimize uncertainty from spatial aggregation, we adopted the non-parametric Thiessen polygon method. While this approach incorporates spatial weighting, it remains sensitive to uneven well distribution. Third, due to the absence of detailed hydrogeological parameters, we were unable to estimate changes in groundwater storage at fine spatial resolutions. This is particularly relevant for confined aquifers, where recovery may be delayed due to long-term compaction effects and limited vertical recharge. Finally, this study focused solely on the NCP due to the intensive effort required to collect and digitize data from printed hydrogeological yearbooks. Expanding this analysis to other regions would require a similar investment in data acquisition and quality control. Nonetheless, our uncertainty analysis (Fig. 3a, b) suggests that these limitations do not compromise the core finding of rapid and regionally significant groundwater recovery in the NCP.

### Data availability

GRACE TWSA products were accessible from the Jet Propulsion Laboratory (JPL, <https://grace.jpl.nasa.gov>) and Center for Space Research (CSR, <https://www.csr.utexas.edu>). Soil moisture products were accessible from the Global Land Data Assimilation System (GLDAS, <https://ldas.gsfc.nasa.gov/gldas/>). All other data used in this study and source data for generating figures are accessible from Zenodo (<https://doi.org/10.5281/zenodo.15797080>)<sup>69</sup>.

### Code availability

Data processing and analysis were conducted using MATLAB. The related code can be found on Zenodo (<https://doi.org/10.5281/zenodo.15797080>)<sup>69</sup>.

### References

1. Scanlon, B. R. et al. Global water resources and the role of groundwater in a resilient water future. *Nat. Rev. Earth Environ.* **4**, 87–101 (2023).
2. Döll, P. et al. Global-scale assessment of groundwater depletion and related groundwater abstractions: Combining hydrological modeling with information from well observations and GRACE satellites. *Water Resour. Res.* **50**, 5698–5720 (2014).
3. Gleeson, T., Wada, Y., Bierkens, M. F. P. & van Beek, L. P. H. Water balance of global aquifers revealed by groundwater footprint. *Nature* **488**, 197–200 (2012).

4. Wada, Y. et al. Global depletion of groundwater resources. *Geophys. Res. Lett.* **37**, L20402 (2010).
5. Jasechko, S. et al. Rapid groundwater decline and some cases of recovery in aquifers globally. *Nature* **625**, 715–721 (2024).
6. Ao, Z. et al. A national-scale assessment of land subsidence in China's major cities. *Science* **384**, 301–306 (2024).
7. Herrera-García, G. et al. Mapping the global threat of land subsidence. *Science* **371**, 34–36 (2021).
8. de Graaf, I. E. M., Gleeson, T., van Beek, L. P. H., Sutanudjaja, E. H. & Bierkens, M. F. P. Environmental flow limits to global groundwater pumping. *Nature* **574**, 90–94 (2019).
9. Condon, L. E. & Maxwell, R. M. Simulating the sensitivity of evapotranspiration and streamflow to large-scale groundwater depletion. *Sci. Adv.* **5**, eaav4574 (2019).
10. Werner, A. D. et al. Seawater intrusion processes, investigation and management: Recent advances and future challenges. *Adv. Water Resour.* **51**, 3–26 (2013).
11. Deines, J. M. et al. Transitions from irrigated to dryland agriculture in the Ogallala Aquifer: Land use suitability and regional economic impacts. *Agric. Water Manag.* **233**, 106061 (2020).
12. Tillman, F. D. & Flynn, M. E. Arizona Groundwater Explorer: interactive maps for evaluating the historical and current groundwater conditions in wells in Arizona, USA. *Hydrogeol. J.* **32**, 645–661 (2024).
13. Buapeng, S. & Foster, S. Controlling groundwater abstraction and related environmental degradation in metropolitan Bangkok – Thailand. Report number: GW-MATe Case Profile Collection 20Affiliation: World Bank (Washington DC) [www.worldbank.org/gwmat](http://www.worldbank.org/gwmat) (2008).
14. Karimi, H. & Alimoradi, S. Impacts of water transfer from Karkheh Dam on rising of groundwater in Dasht-e-Abass Plain, Ilam Province. *Res. Earth Sci.* **8**, 33–44 (2017).
15. Alam, S., Gebremichael, M., Li, R., Dozier, J. & Lettenmaier, D. P. Can managed aquifer recharge mitigate the groundwater overdraft in California's central valley?. *Water Resour. Res.* **56**, e2020WR027244 (2020).
16. Ulibarri, N., Escobedo Garcia, N., Nelson, R. L., Cravens, A. E. & McCarty, R. J. Assessing the feasibility of managed aquifer recharge in California. *Water Resour. Res.* **57**, e2020WR029292 (2021).
17. Long, D. et al. South-to-north water diversion stabilizing Beijing's groundwater levels. *Nat. Commun.* **11**, 3665 (2020).
18. Scanlon, B. R., Reedy, R. C., Faunt, C. C., Pool, D. & Uhlman, K. Enhancing drought resilience with conjunctive use and managed aquifer recharge in California and Arizona. *Environ. Res. Lett.* **11**, 035013 (2016).
19. Tang, W. et al. Land subsidence and rebound in the Taiyuan basin, northern China, in the context of inter-basin water transfer and groundwater management. *Remote Sens. Environ.* **269**, 112792 (2022).
20. Martínez-Santos, P., Castaño-Castaño, S. & Hernández-Espriú, A. Revisiting groundwater overdraft based on the experience of the Mancha Occidental Aquifer, Spain. *Hydrogeol. J.* **26**, 1083–1097 (2018).
21. Monir, M. M. & Sarker, S. C. Analyzing post-2000 groundwater level and rainfall changes in Rajasthan, India, using well observations and GRACE data. *Heliyon* **10**, e24481 (2024).
22. Zheng, C. et al. Can China cope with its water crisis?—Perspectives from the North China Plain. *Groundwater* **48**, 350–354 (2010).
23. Liu, J., Zheng, C., Zheng, L. & Lei, Y. Ground water sustainability: methodology and application to the North China plain. *Groundwater* **46**, 897–909 (2008).
24. Yang, H. et al. Evolution of groundwater level in the North China Plain in the past 40 years and suggestions on its overexploitation treatment. *Geol. China* **48**, 1142–1155 (2021).
25. Cao, G., Zheng, C., Scanlon, B. R., Liu, J. & Li, W. Use of flow modeling to assess sustainability of groundwater resources in the North China Plain. *Water Resour. Res.* **49**, 159–175 (2013).
26. Yang, W. et al. Human intervention will stabilize groundwater storage across the north China plain. *Water Resour. Res.* **58**, e2021WR030884(2022).
27. Zhang, C. et al. Sub-regional groundwater storage recovery in North China Plain after the South-to-North water diversion project. *J. Hydrol.* **597**, 126156 (2021).
28. Zhang, C. et al. The Effectiveness of the South-to-North water diversion middle route project on water delivery and groundwater recovery in north china plain. *Water Resour. Res.* **56**, e2019WR026759 (2020).
29. Li, X., Ye, S.-Y., Wei, A.-H., Zhou, P.-P. & Wang, L.-H. Modelling the response of shallow groundwater levels to combined climate and water-diversion scenarios in Beijing-Tianjin-Hebei Plain, China. *Hydrogeol. J.* **25**, 1733–1744 (2017).
30. Dong, L. et al. Shifting agricultural land use and its unintended water consumption in the North China Plain. *Sci. Bull.* **69**, 3968–3977 (2024).
31. Chen, Y., Yin, G. & Liu, K. Regional differences in the industrial water use efficiency of China: the spatial spillover effect and relevant factors. *Resour. Conserv. Recycl.* **167**, 105239 (2021).
32. Chen, F., Ding, Y., Tang, S., Ding, L. & Yang, Y. Practice and effect analysis of river-lake ecological water supplement and groundwater recharge in the North China region. *China Water Resour.* **7**, 36–39 (2021).
33. National Bureau of Statistics. China rural statistical yearbook (2005–2024).
34. Butler, J. J. Jr, Whitemore, D. O., Wilson, B. B. & Bohling, G. C. A new approach for assessing the future of aquifers supporting irrigated agriculture. *Geophys. Res. Lett.* **43**, 2004–2010 (2016).
35. Zheng, H., Liu, Y. & Zhao, J. Understanding water rights and water trading systems in China: a systematic framework. *Water Secur.* **13**, 100094 (2021).
36. Hai River basin Water Authority. Hai River Water Resources Bulletin (2005–2023).
37. Pérez-Blanco, C. D., Loch, A., Ward, F., Perry, C. & Adamson, D. Agricultural water saving through technologies: a zombie idea. *Environ. Res. Lett.* **16**, 114032 (2021).
38. Noori, R. et al. Anthropogenic depletion of Iran's aquifers. *Proc. Natl. Acad. Sci.* **118**, e2024221118 (2021).
39. Alattar, M. H. Mapping groundwater dynamics in Iraq: integrating multi-data sources for comprehensive analysis. *Model. Earth Syst. Environ.* **10**, 4375–4385 (2024).
40. Caló, F. et al. DInSAR-based detection of land subsidence and correlation with groundwater depletion in Konya Plain, Turkey. *Remote Sens.* **9**, 83 (2017).
41. Massoud, E. C., Liu, Z., Shaban, A. & Hage, M. E. Groundwater depletion signals in the Beqaa Plain, Lebanon: evidence from GRACE and Sentinel-1 data. *Remote Sens.* **13**, 915(2021).
42. Brückner, F. et al. Causes and consequences of long-term groundwater overabstraction in Jordan. *Hydrogeol. J.* **29**, 2789–2802 (2021).
43. van Rooyen, J. D., Watson, A. P. & Miller, J. A. Combining quantity and quality controls to determine groundwater vulnerability to depletion and deterioration throughout South Africa. *Environ. Earth Sci.* **79**, 255 (2020).
44. Jasechko, S. & Perrone, D. California's central valley groundwater wells run dry during recent drought. *Earth's Future* **8**, e2019EF001339 (2020).
45. Scanlon, B. R. et al. Groundwater depletion and sustainability of irrigation in the US high plains and central valley. *Proc. Natl. Acad. Sci.* **109**, 9320–9325 (2012).

46. Butler, J. J. Jr, Whittemore, D. O., Wilson, B. B. & Bohling, G. C. Sustainability of aquifers supporting irrigated agriculture: a case study of the High Plains aquifer in Kansas. *Water Int.* **43**, 815–828 (2018).
47. MacDonald, A. M. et al. Groundwater quality and depletion in the Indo-Gangetic Basin mapped from in situ observations. *Nat. Geosci.* **9**, 762–766 (2016).
48. Faunt, C. C. et al. Groundwater sustainability and land subsidence in California's central valley. *Water* **16**, 1189 (2024).
49. Furman, A. & Abbo, H. In *Water Policy in Israel: Context, Issues and Options* (ed Nir Becker) 125–136 (Springer Netherlands, 2013).
50. Shumilova, O., Tockner, K., Thieme, M., Koska, A. & Zarfl, C. Global water transfer megaprojects: a potential solution for the water-food-energy nexus? *Front. Environ. Sci.* **6**, <https://doi.org/10.3389/fenvs.2018.00150> (2018).
51. MacAllister, D. J., Krishan, G., Basharat, M., Cuba, D. & MacDonald, A. M. A century of groundwater accumulation in Pakistan and northwest India. *Nat. Geosci.* **15**, 390–396 (2022).
52. Chauhan, T., Devanand, A., Roxy, M. K., Ashok, K. & Ghosh, S. River interlinking alters land-atmosphere feedback and changes the Indian summer monsoon. *Nat. Commun.* **14**, 5928 (2023).
53. Tillman, F. D. & Leake, S. A. Trends in groundwater levels in wells in the active management areas of Arizona, USA. *Hydrogeol. J.* **18**, 1515–1524 (2010).
54. Jacobs, K. L. & Holway, J. M. Managing for sustainability in an arid climate: lessons learned from 20 years of groundwater management in Arizona, USA. *Hydrogeol. J.* **12**, 52–65 (2004).
55. Ganguly, S. & Ganguly, S. Implementation of managed aquifer recharge techniques in India. *Curr. Sci.* **121**, 641–650 (2021).
56. Ebrahim, G. Y., Lautze, J. F. & Villholth, K. G. Managed aquifer recharge in africa: taking stock and looking forward. *Water* **12**, 1844 (2020).
57. Standen, K., Costa, L. R. D. & Monteiro, J.-P. In-channel managed aquifer recharge: a review of current development worldwide and future potential in Europe. *Water* **12**, 11 (2020).
58. Jones, E., Qadir, M., van Vliet, M. T. H., Smakhtin, V. & Kang, S. -m The state of desalination and brine production: a global outlook. *Sci. Total Environ.* **657**, 1343–1356 (2019).
59. Smith, K., Liu, S., Hu, H.-Y., Dong, X. & Wen, X. Water and energy recovery: the future of wastewater in China. *Sci. Total Environ.* **637–638**, 1466–1470 (2018).
60. Nan, T. et al. Evaluation of shallow groundwater dynamics after water supplement in North China Plain based on attention-GRU model. *J. Hydrol.* **625**, 130085 (2023).
61. Bai, L. et al. Quantifying the influence of long-term overexploitation on deep groundwater resources across Cangzhou in the North China Plain using InSAR measurements. *J. Hydrol.* **605**, 127368 (2022).
62. Sen, P. K. Estimates of the regression coefficient based on Kendall's Tau. *J. Am. Stat. Assoc.* **63**, 1379–1389 (1968).
63. Theil, H. In *Henri Theil's Contributions to Economics and Econometrics: Econometric Theory and Methodology* (eds. Baldev Raj & Johan Koerts) 345–381 (Springer Netherlands, 1992).
64. Mann, H. B. Nonparametric tests against trend. *Econometrica* **13**, 245–259 (1945).
65. Su, G. et al. Spatiotemporal evolution characteristics of land subsidence caused by groundwater depletion in the North China plain during the past six decades. *J. Hydrol.* **600**, 126678 (2021).
66. Yu, X., Wang, G., Hu, X., Liu, Y. & Bao, Y. Land Subsidence in Tianjin, China: Before and after the South-to-North Water Diversion. *Remote Sensing* **15**, 1647 (2023).
67. Guo, H. et al. Land subsidence and its affecting factors in Cangzhou, North China Plain. *Front. Environ. Sci.* **10** (2022).
68. Cao, G., Scanlon, B. R., Han, D. & Zheng, C. Impacts of thickening unsaturated zone on groundwater recharge in the North China plain. *J. Hydrol.* **537**, 260–270 (2016).
69. Xu, Y., Long, D. & Cui, Y. Unprecedented large-scale aquifer recovery through human intervention. <https://doi.org/10.5281/zenodo.15797080> (2025).

## Acknowledgements

This study was supported by the National Key Research and Development Program of China (Grant No. 2021YFB3900604 to D.L. and Y.C.), the National Natural Science Foundation of China (Grant Nos. 52325901 to D.L. and 52079065 to D.L.), and the World Bank China Water PASA program to D.L.

## Author contributions

D.L., Y.X., and Y.J.C. developed the concept and methodology of this study. D.L., Y.X., and Y.J.C. performed the data processing and analysis with support from all other authors. D.L., Y.X., Y.J.C., Y.H.C., J.J.B., L.D., L.W., D.Y.L., Y.W., L.H., G.B., B.L., S.W., X.N., Y.C., C.C., Y.M., Y.Q., J.W., H.W., and B.R.S. discussed the results and improved the writing of this manuscript.

## Competing interests

The authors declare no competing interests.

## Additional information

**Supplementary information** The online version contains supplementary material available at <https://doi.org/10.1038/s41467-025-62719-5>.

**Correspondence** and requests for materials should be addressed to Di Long.

**Peer review information** *Nature Communications* thanks Juan Antonio Torres-Martinez, Ian Holman and the other anonymous reviewer(s) for their contribution to the peer review of this work. A peer review file is available.

**Reprints and permissions information** is available at <http://www.nature.com/reprints>

**Publisher's note** Springer Nature remains neutral with regard to jurisdictional claims in published maps and institutional affiliations.

**Open Access** This article is licensed under a Creative Commons Attribution-NonCommercial-NoDerivatives 4.0 International License, which permits any non-commercial use, sharing, distribution and reproduction in any medium or format, as long as you give appropriate credit to the original author(s) and the source, provide a link to the Creative Commons licence, and indicate if you modified the licensed material. You do not have permission under this licence to share adapted material derived from this article or parts of it. The images or other third party material in this article are included in the article's Creative Commons licence, unless indicated otherwise in a credit line to the material. If material is not included in the article's Creative Commons licence and your intended use is not permitted by statutory regulation or exceeds the permitted use, you will need to obtain permission directly from the copyright holder. To view a copy of this licence, visit <http://creativecommons.org/licenses/by-nc-nd/4.0/>.

© The Author(s) 2025